RSC Advances



PAPER

View Article Online
View Journal | View Issue



Cite this: RSC Adv., 2024, 14, 26516

First-principles calculations to investigate the impact of fluorine doping on electrochemical properties of Li-rich Li₂MnO₃ layered cathode materials

Xiang-Ming Zeng,^{abc} Jing Liu,^d Jiang-Bin Su,^{ab} Fa-Hui Wang,^{ab} Yan-Bing Li,^{ab} Chang-Jun Zhan,^{ab} Ming Liu,^{ab} Run-Sheng Wu,^{abc} Jun-Ping Hu ^{be} and Feng Zheng ⁵

Li-rich layered oxides are promising candidates for high-capacity Li-ion battery cathode materials. In this study, we employ first-principles calculations to investigate the effect of F doping on Li-rich Li_2MnO_3 layered cathode materials. Our findings reveal that both Li_2MnO_3 and $\text{Li}_2\text{MnO}_{2.75}\text{F}_{0.25}$ exhibit significant volume changes (greater than 10%) during deep delithiation, which could hinder the cycling of more Li ions from these two materials. For Li_2MnO_3 , it is observed that oxygen ions lose electrons to compensate for charge during the delithiation process, leading to a relatively high voltage plateau. After F doping, oxidation occurs in both the cationic (Mn) and anionic (O) components, resulting in a lower voltage plateau at the beginning of the charge, which can be attributed to the oxidation of Mn^{3+} to Mn^{4+} . Additionally, F doping can somewhat suppress the release of oxygen in Li_2MnO_3 , improving the stability of anionic oxidation. However, the increase of the activation barriers for Li diffusion can be observed after F doping, due to stronger electrostatic interactions between F⁻ and Li⁺, which adversely affects the cycling kinetics of $\text{Li}_2\text{MnO}_{2.75}\text{F}_{0.25}$. This study enhances our understanding of the impact of F doping in Li_2MnO_3 based on theoretical calculations.

Received 8th July 2024 Accepted 12th August 2024

DOI: 10.1039/d4ra04925j

rsc.li/rsc-advances

Introduction

Li-ion batteries (LIBs) are extensively used in portable devices for their long cycle life, safety and high energy density.¹ However, entering new areas, like electric vehicles market, demands LIBs with higher energy density.²-⁴ Cathode materials, a key component of LIBs, are seen as a significant bottleneck in developing high-energy-density LIBs.⁵ Current transitional cathodes, such as LiCoO₂ and LiFePO₄, are approaching their theoretical limits. Consequently, the need for new cathode materials with higher energy density has become more urgent than ever. Recently, Li-rich oxides have emerged as a promising

Elemental doping is regarded as a viable strategy to enhance the electrochemical properties of Li-rich oxides. For instance, Wang *et al.* showed that F-doping Li[Li_{0.133}Mn_{0.467}Ni_{0.2}Co_{0.2}]O₂ suppresses voltage decay and enhances capacity retention compared to its undoped counterpart.¹⁸ Additionally, Vanaphuti *et al.* demonstrated that co-doping Na and F into Li-rich Mn-base oxides improves structural stability and mitigates oxygen loss.¹⁹ Mao *et al.* also proposed an effective, straightforward, and scalable co-doping strategy with trace amounts of Fe and F to enhance the rate capability and cycling performance of high-Ni Li-rich layered oxides.²⁰ These results show that F is a significant anion in the elemental doping of Li-rich materials. However, most studies focus on experimental analysis to highlight the key role of F doping in performance enhancement. There is a lack of exploration into the underlying mechanisms

solution to achieve this goal.^{6,7} Thanks to cumulative cationic and anionic redox reactions, these materials can achieve capacities exceeding 250 mA h g⁻¹.⁸⁻¹⁰ Nevertheless, these materials have drawbacks such as significant voltage decay, ^{10,11} voltage hysteresis, ^{12,13} poor rate capability, ¹⁴ and capacity loss ¹⁵ during cycling, due to the structural transformation of host materials during the oxygen redox. ^{10,12,13} Therefore, numerous measures have been implemented to improve their structural stability. ¹⁵⁻¹⁷

[&]quot;School of New Energy Science and Engineering, Xinyu University, Xinyu 338004, China

^bJiangxi Provincial Key Laboratory of Power Batteries & Energy Storage Materials, Xinyu University, Xinyu 338004, China

Jiangxi Lithium Battery New Material Industry Technology Institute, Jiangxi Yingxing Lithium Battery New Materials Industrial Technology Institute Co., Ltd, Xinyu 338004, China

^dLibrary, Xinyu University, Xinyu 338004, China

^eNanchang Key Laboratory of Photoelectric Conversion and Energy Storage Materials, Nanchang Institute of Technology, Nanchang 330099, China

School of Science, Jimei University, Xiamen 361021, China. E-mail: fzheng@jmu.edu. cn

of F doping's effect on the electrochemical properties of Li-rich materials through theoretical calculations. In this study, using first-principles calculations, we investigate the impact of F doping on the electrochemical performance of Li-rich Li₂MnO₃, including voltage profile, redox reaction, structural stability, and ionic conductivity. Our results deepen the understanding of F doping's role in Li-rich materials.

2. Computational methods

The present calculations are carried out by using the projectoraugmented wave (PAW)21 representations within density functional theory (DFT) as implemented in the Vienna Ab initio Simulation Package (VASP).22,23 The exchange and correlation energy is treated within the spin-polarized generalized gradient approximation (GGA) and parameterized by Perdew-Burke-Ernzerhof formula (PBE).24 The effects due to the localization of the d electrons of the transition metal ions were taken into account with the GGA + U approach of Dudarev et al.25 An effective single parameter U-J of 5.0 eV is used for Mn, which has been proved to be a good approximation in Mn-based compounds.26,27 Wave functions are expanded in plane waves up to a kinetic energy cut-off of 550 eV. Brillouin-zone integrations are approximated by using special k-point sampling of Monkhorst–Pack scheme²⁸ with a k-point mesh resolution of 2π \times 0.03 Å⁻¹. Lattice vectors together with the atomic coordinates were fully relaxed until the force on each atom is less than 0.01 eV Å^{-1} .

The relative stability of LixHost polymorphs at each Li composition x was evaluated by

$$\Delta E_{\rm f} = E({\rm Li}_x {\rm Host}) - \left[\frac{x}{2} E({\rm Li}_2 {\rm Host}) + \left(1 - \frac{x}{2}\right) E({\rm Host})\right] \quad (1)$$

where E is the calculated total energy for a given structure. The average voltage (V) versus Li/Li⁺ was calculated as

$$V = \frac{E_{\text{tot}}(\text{Li}_{x_2}\text{Host}) - E_{\text{tot}}(\text{Li}_{x_1}\text{Host}) - (x_2 - x_1)E_{\text{tot}}[\text{Li}]}{(x_2 - x_1)e}$$
 (2)

where x_2 and x_1 are the Li composition before and after the lithium extraction from the host structure, respectively.

The reaction energy associated with the formation of oxygen vacancy in Li₂MnO₃ and Li₂MnO_{2,75}F_{0,25} was calculated by

$$\Delta H = \frac{E_{\text{tot}} \left(\text{Li}_x \text{MnO}_{3-y} \right) + \left(\frac{y}{2} \right) E(\text{O}_2) - E_{\text{tot}} \left(\text{Li}_x \text{MnO}_3 \right)}{v/2}$$
(3)

and

$$\Delta H = \frac{E_{\text{tot}} \left(\text{Li}_x \text{MnO}_{2.75-y} \text{F}_{0.25} \right) + \left(\frac{y}{2} \right) E(\text{O}_2) - E_{\text{tot}} \left(\text{Li}_x \text{MnO}_{2.75} \text{F}_{0.25} \right)}{y/2}$$
(4)

The total energy of a single oxygen molecule $(E(O_2))$ was calculated in a 20 \times 20 \times 20 Å periodic box, and the correction proposed by Ceder et al.²⁹ was then added to $E(O_2)$.

The activation barriers for the Li migration in Li₂MnO₃ and Li₂MnO_{2.75}F_{0.25} were calculated using the climbing nudged

elastic band (NEB) method³⁰ in a $2 \times 1 \times 2$ supercell containing 16 formula units. For the NEB calculations, the standard GGA functional was employed, and the lattice constants of a given structure were fixed as their equilibrium values, with all the internal degrees of freedom fully relaxed.

3. Results and discussion

Effect of F-doping on the voltage profile and volume change of Li₂MnO₃

The crystal structure of Li₂MnO₃ considered in this study has a monoclinic symmetry with C2/m space group and includes 12 O atoms at 4i and 8j sites in the unit cell. We replace one of the O atoms with F (substituting O at 8j site is more stable) to construct F-doped Li₂MnO_{2.75}F_{0.25} structure as shown in Fig. 1. The increase in volume following F doping is shown in Table 1, which indicates a 2.38% volume expansion. We also examined the impact of F-doping on the voltage profile of Li₂MnO₃. To calculate the theoretical voltage, the formation energies of delithiated structures were first investigated based on the eqn (1). For Li_xMnO₃, all possible Li distributions are considered, as shown in Fig. 2(a). The lowest energy Li_xMnO₃ compounds were then used to replace O with F to construct F-doped Lix-MnO_{2.75}F_{0.25}, and their formation energies were calculated, as shown in Fig. 2(b). The delithiated structures that lie on the convex hull indicated stable intermediate phases. For Li2MnO3, two stable intermediate phases, Li_{0.5}MnO₃ and Li_{0.125}MnO₃, are found, which is consistent with previous work.31 For the Fdoped Li₂MnO_{2.75}F_{0.25}, the phases of Li_{1.75}MnO_{2.75}F_{0.25}, Li_{0.5}- $MnO_{2.75}F_{0.25}$ and $Li_{0.125}MnO_{2.75}F_{0.25}$ lie on the convex hull. Our

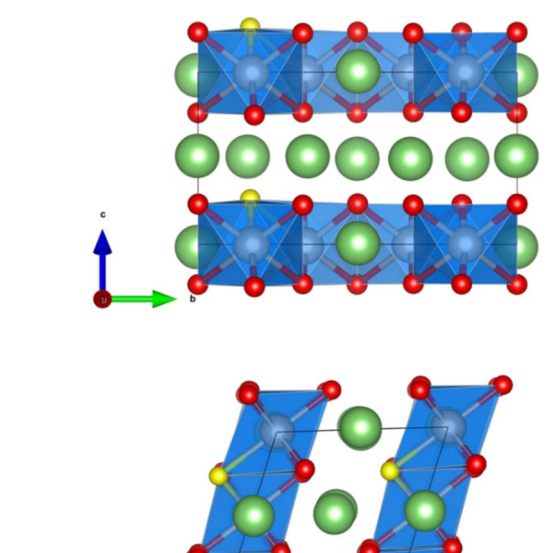


Fig. 1 The crystal structure of $Li_2MnO_{2.75}F_{0.25}$. The Li and O atoms are denoted by green and red spheres, respectively. The substituted O atom by F is shown as a yellow sphere. The MnO₆ octahedra are highlighted in blue.

Table 1 The lattice parameters of Li₂MnO₃ and Li₂MnO_{2.75}F_{0.25}

	a, b, c (Å)	β (°)	V (ų per f.u.)
$\begin{array}{l} \text{Li}_2\text{MnO}_3\\ \text{Li}_2\text{MnO}_{2.75}\text{F}_{0.25} \end{array}$	5.01, 8.66, 5.08	109.48	51.99
	5.04, 8.80, 5.09	109.12	53.23

calculated results show that these three stable delithiated Li_x -MnO_{2.75}F_{0.25} compounds all have F substituting the O 8j sites. Using these stable phases, we calculated the theoretical average voltages for Li_2 MnO₃ and Li_2 MnO_{2.75}F_{0.25} using eqn (2), as shown in Fig. 2(c). For Li_2 MnO₃, a long voltage plateau at around 4.41 V is observed, which aligns well with experimental results.³² When more Li ions were extracted (0.5 > x > 0), two higher voltage plateaus at 5.52 and 5.69 V appear. After F-doping, a short plateau (2.0 > x > 1.75) is observed, corresponding to a lower voltage of 3.50 V. As more Li ions were extracted, a long plateau can be seen at 4.39 V, followed by two higher plateaus between x = 0.5 and x = 0. We will discuss the

changes in oxidation potential between Li₂MnO₃ and Li₂-MnO_{2.75}F_{0.25} during delithiation later in this paper.

We also investigated the volume changes of Li_2MnO_3 and $\text{Li}_2\text{MO}_{2.75}\text{F}_{0.25}$ during delithiation, as shown in Fig. 2(d). For the first Li extraction, the volume changes of Li_2MnO_3 and $\text{Li}_2\text{-MnO}_{2.75}\text{F}_{0.25}$ are -1.1% and -2.7%, respectively. With further Li extraction ($\text{Li}_{0.5}\text{MnO}_3$ and $\text{Li}_{0.5}\text{MnO}_{2.75}\text{F}_{0.25}$), the calculated volume changes are -12.8% and -13.7%. Such substantial volume change could hinder the cycling of more Li ions from Li_2MnO_3 and $\text{Li}_2\text{MnO}_{2.75}\text{F}_{0.25}$, which suggests their structural instability upon deep delithiation.

3.2 Effect of F-doping on oxidation of Li₂MnO₃

Fig. 3(a) shows the calculated projected density of states (PDOS) for Li_xMnO_3 , indicating that Li_2MnO_3 is a semiconductor with a band gas of ~ 1.32 eV. The valence band maximum is dominated by O 2p non-bonding states, attributed to a Li–O–Li configuration in the Li_2MnO_3 structure. As Li ions are extracted, the Fermi level shifts towards lower energy, leading to the gradual extraction of electrons from non-bonding O 2p states. Therefore, the observed voltage plateaus of 4.41, 5.52 and 5.69 V

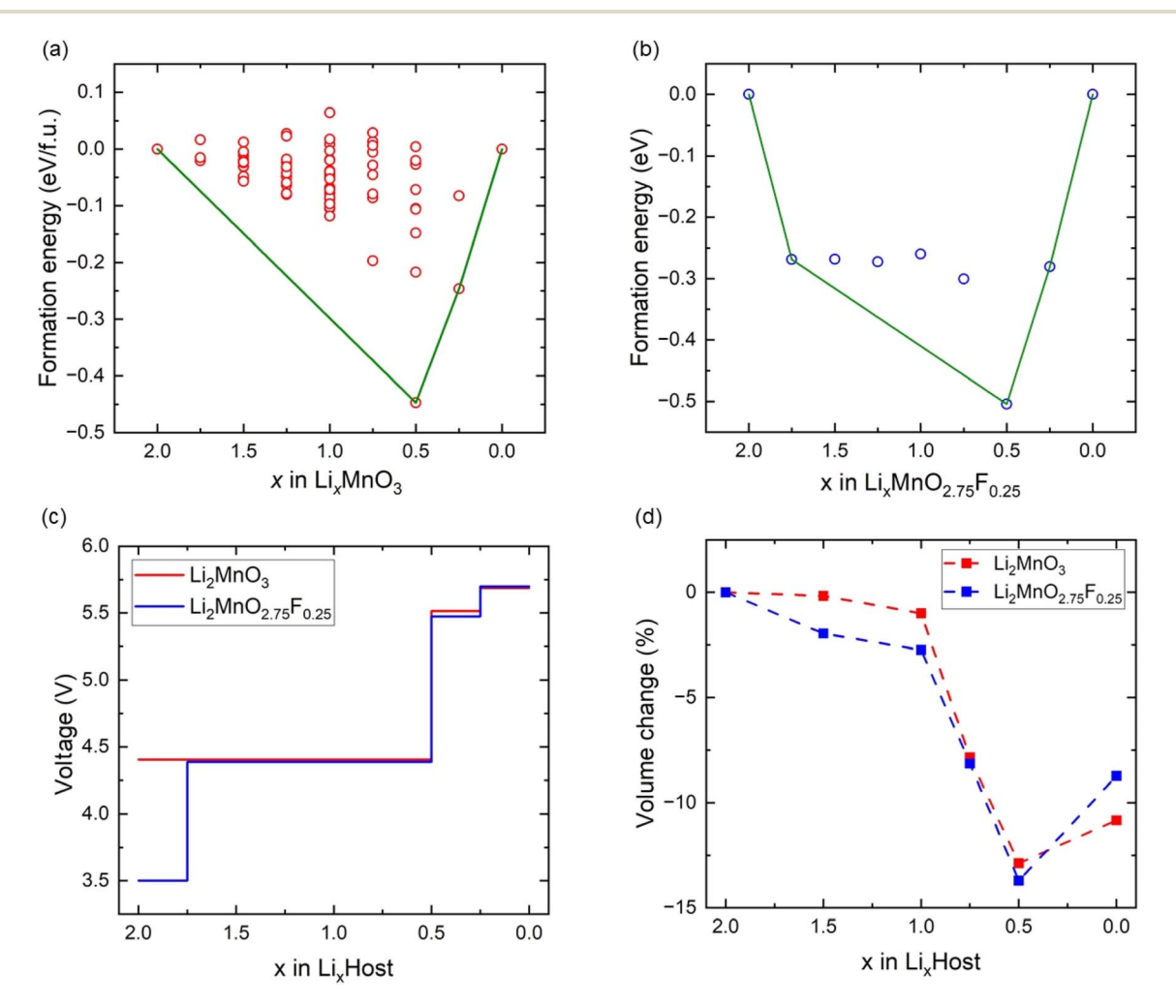


Fig. 2 The formation energies (a) Li_2MnO_3 and (b) $\text{Li}_2\text{MnO}_{2.75}\text{F}_{0.25}$. (c) The voltage profiles of Li_2MnO_3 and $\text{Li}_2\text{MnO}_{2.75}\text{F}_{0.25}$. (d) The volume change of Li_2MnO_3 and $\text{Li}_2\text{MnO}_{2.75}\text{F}_{0.25}$.

Paper

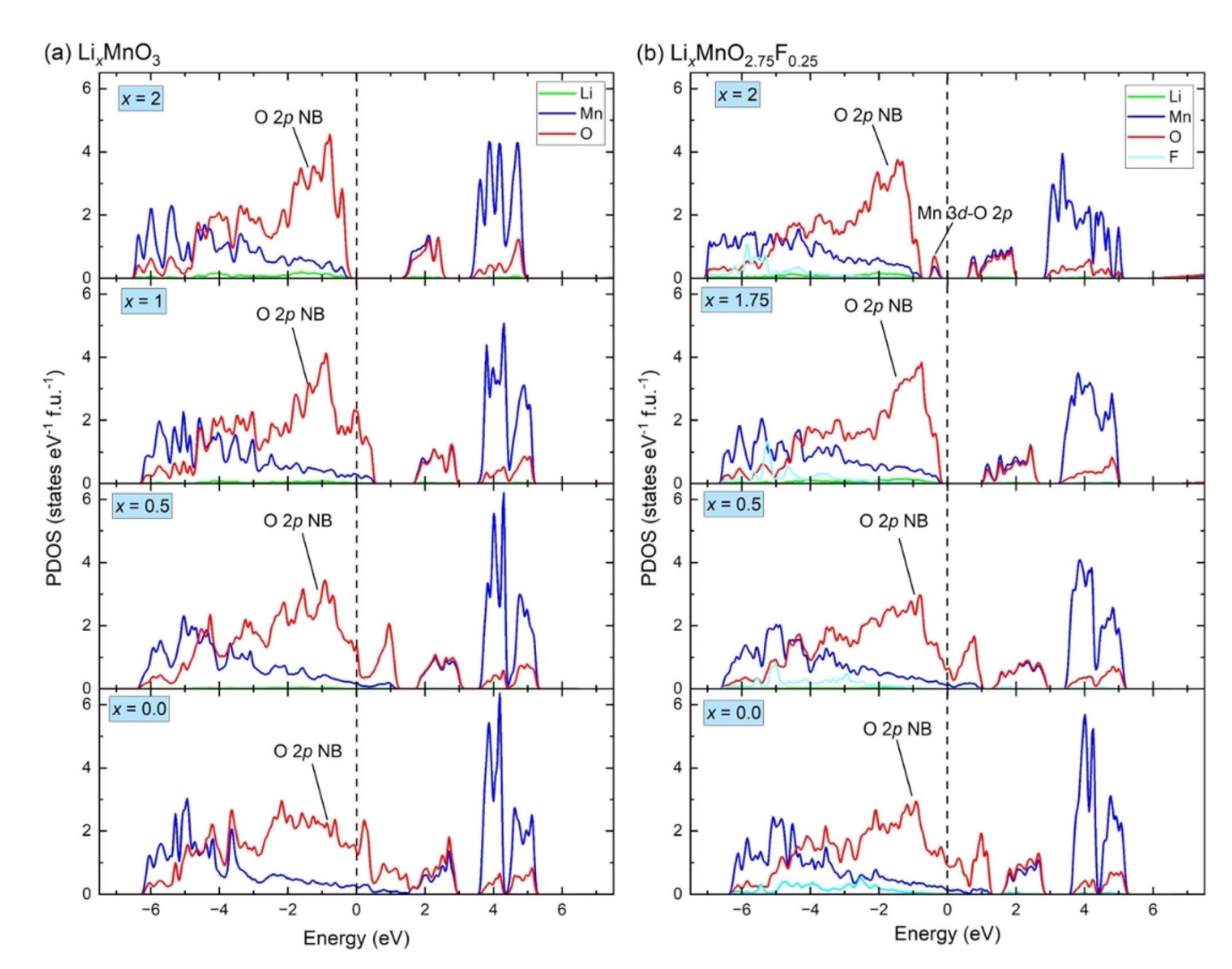


Fig. 3 The density of states for (a) $\text{Li}_x \text{MnO}_3$ and (b) $\text{Li}_x \text{MnO}_{2.75} \text{F}_{0.25}$. The non-bonding O 2p states is denoted as "O 2p NB", the hybridized Mn 3d–O 2p states is denoted as "Mn 3d–O 2p".

for Li_2MnO_3 (Fig. 2(c)) all correspond to oxygen oxidation. These results are consistent with the calculated magnetic moments for Li_2MnO_3 (Fig. 4(a) and (b)). In Li_2MnO_3 (4 Mn atoms and 12 O atoms per unit cell), all four Mn atoms display a magnetic moment of approximately 3.0, indicative of a valence state of +4 (3d³, high-spin state $e_g^0t_{2g}^3$) as depicted in Fig. 4(c). Upon Li ion extraction, the magnetic moment of Mn remains almost unchanged, suggesting that Mn does not participate in oxidation. As illustrated in Fig. 4(b), all 12 O atoms in Li_2MnO_3 exhibit a magnetic moment of approximately 0, indicating a pristine valence state of -2 for O. During the delithiation process, the magnetic moment of O increases, indicating oxygen oxidation.

In F-doped Li₂MnO_{2.75}F_{0.25}, the valence band maximum is dominated by hybridized Mn 3d–O 2p states, as shown in Fig. 3(b). During delithiation from Li₂MnO_{2.75}F_{0.25} to Li_{1.75}-MnO_{2.75}F_{0.25}, the hybridized Mn 3d–O 2p states shift to higher energy (above Fermi level), indicating that Mn atoms lose electrons to maintain charge balance. This observation aligns with the magnetic moment calculations depicted in Fig. 4(d). In

Li₂MnO_{2.75}F_{0.25}, one of the four Mn atoms exhibits a magnetic moment of about 4.0, indicative of a valence state of +3 (3d⁴, high-spin state $e_g^1t_{2g}^3$) as shown in Fig. 4(c). At x=1.75, oxidation from Mn³⁺ to Mn⁴⁺ occurs. Consequently, a lower voltage plateau of 3.50 V is observed between Li₂MnO_{2.75}F_{0.25} and Li_{1.75}MnO_{2.75}F_{0.25}, as illustrated in Fig. 2(c). With further delithiation (x < 1.75), non-bonding O 2p states begin to be extracted, as seen in Fig. 3(b) and 4(e), indicating electron loss from oxygen ions. The oxygen oxidation process occurring in Li₂MnO_{2.75}F_{0.25} exhibits parallels to that observed in Li₂MnO₃, resulting in similar voltage plateaus at x < 1.75 (Fig. 2(c)). The magnetic moment of F remains close to 0 in Li₂MnO_{2.75}F_{0.25} upon delithiation, showing that F does not participate in oxidation, as depicted in Fig. 4(f).

We also investigated the effect of F doping on the stability of oxygen redox in $\text{Li}_x \text{MnO}_3$, particularly concerning the formation of O vacancy (ΔE). As shown in Fig. 5, the ΔE values decrease monotonically with the reduction in Li concentration, suggesting a downward trend in stability of $\text{Li}_x \text{MnO}_3$ as x decrease. The ΔE values become negative at x=1.5, indicating that the

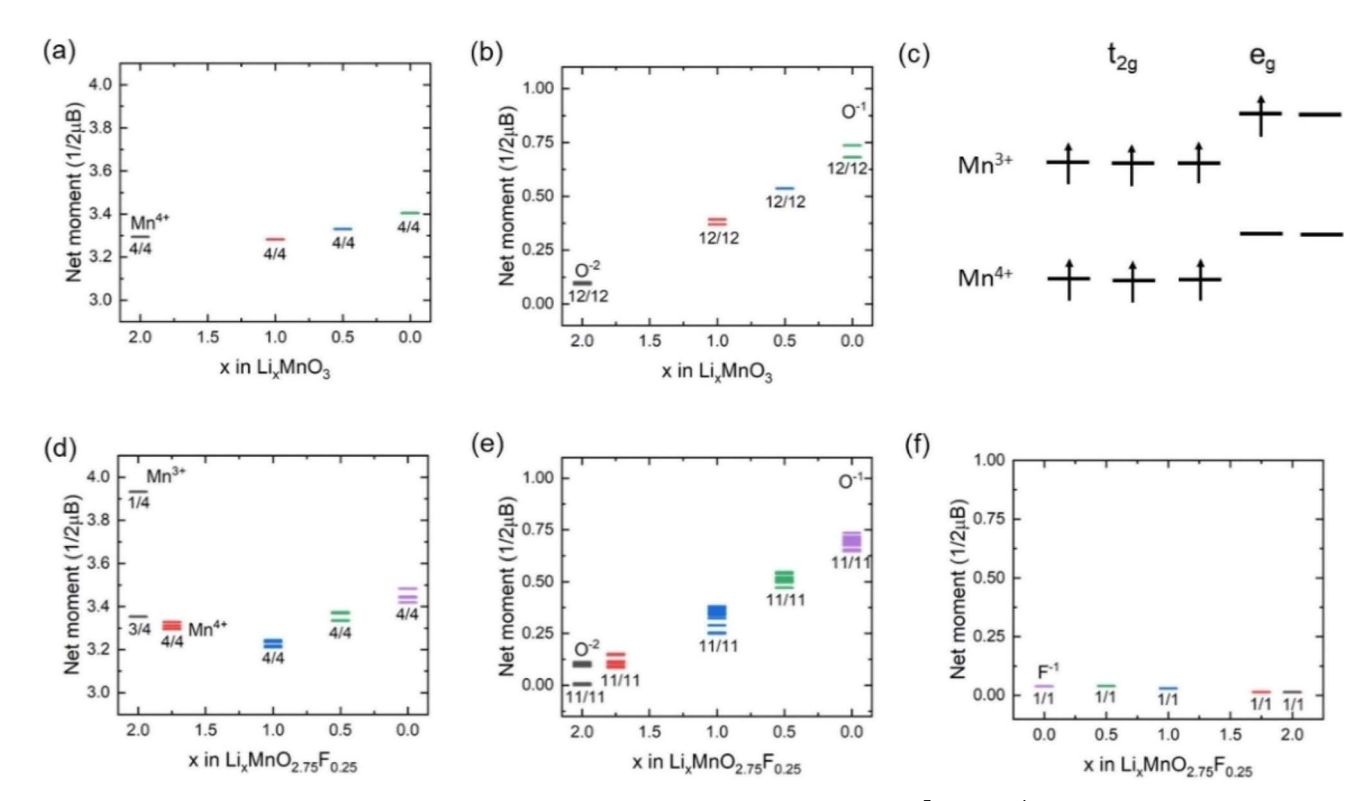


Fig. 4 Magnetic moment variation of (a) Mn and (b) O in Li_2MnO_3 . (c) Schematic diagrams of Mn^{3+} and Mn^{4+} . Corresponding magnetic moment variation of (d) Mn, (e) O and (f) F in $\text{Li}_2\text{MnO}_{2.75}\text{F}_{0.25}$.

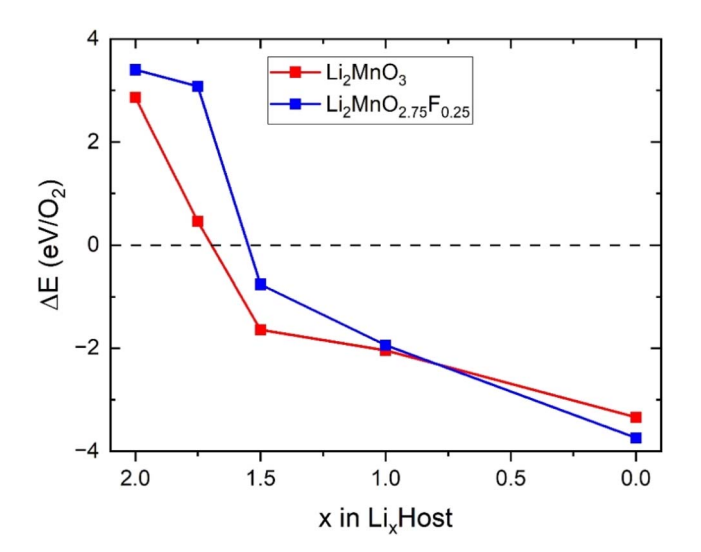


Fig. 5 Calculated formation energy for the reaction of O_2 in Li_2MnO_3 and $Li_2MnO_{2.75}F_{0.25}$ during delithiation.

oxygen release reaction occurs spontaneously in delithiated $\text{Li}_{1.5}\text{MnO}_3$, which is agreed well with previous calculations.³³ Compared to Li_2MnO_3 , smaller values of ΔE can be observed in $\text{Li}_2\text{MnO}_{2.75}\text{F}_{0.25}$ at x < 1.0, suggesting that F doping can somewhat suppress oxygen release. This phenomenon can be attributed to the F doping inducting a minor fraction of Mn to undergo oxidation, which in turn attenuate the oxidation of oxygen and enhances its stability.

Since cation migration is recognized as a leading cause of voltage decay and hysteresis, 10-13 we investigated the effect of Fdoping on Mn migration during deep charge. First, we constructed a $2 \times 1 \times 2$ supercell with 16 formula units and moved one Mn ion to the Li layer in the deeply delithiated state Li_{0.5}MnO₃. After structural optimization, we found that O-O dimers form in this Li_{0.5}MnO₃ with Mn migration, resulting in lower energy compared to pristine $\text{Li}_{0.5}\text{MnO}_3$ ($\Delta E = 67 \text{ meV}$ per atom). This suggests that the deep oxygen oxidation leads to O-O dimer formation and Mn migration, consistent with previous calculations.34 When considering F doping, Mn migration and O-O dimer formation also occur, with the energy of the migrated Mn structure being lower (~70 meV per atom) than that of pristine Li_{0.5}MnO_{2.75}F_{0.25}. These calculated results indicate that F-doping cannot suppress Mn migration at deep charge.

3.3 Effect of F-doping on ionic diffusion

Climbing NEB calculations were used to investigate Li diffusion in Li_2MnO_3 and $\text{Li}_2\text{MnO}_{2.75}\text{F}_{0.25}$, assessing the impact of F-doping on diffusion kinetics. Previous calculations identified two types of Li^+ migration between the neighboring Li and LiMn_2 layers, and three pathways within Li layers. We selected two of these pathways to study the effect of F-doping on ionic diffusion: path 1 involves Li^+ migration from the 4h site to the 2c site in the Li planes (Fig. 6(a)), and path 2 involves Li^+ migration from the 4h site to the 2b site from Li to LiMn_2 layers (Fig. 6(b)). The calculated activation barriers (E_a) along these

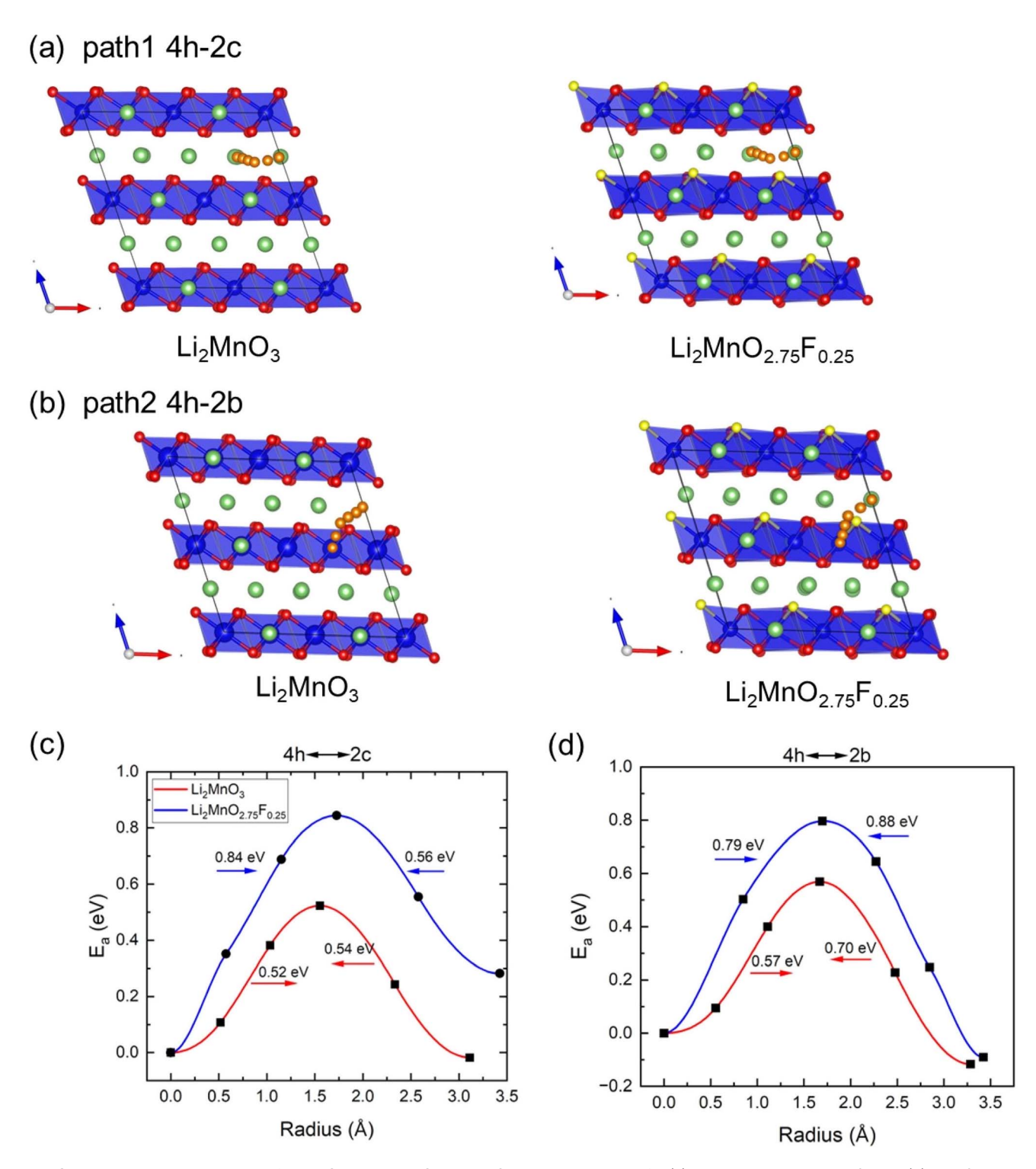


Fig. 6 Calculated kinetic properties of Li_2MnO_3 and $\text{Li}_2\text{MnO}_{2.75}\text{F}_{0.25}$. Schematic diagrams for (a) path 1 between 4h and 2c and (b) path 2 between 4h and 2b for Li_2MnO_3 and $\text{Li}_2\text{MnO}_{2.75}\text{F}_{0.25}$. Calculated activation barrier along (c) path 1 and (d) path 2. The Li and O atoms are denoted by green and red spheres, respectively. The yellow sphere is the substituted O by F atoms. MnO_6 octahedron is colored in blue. Li diffusion paths are represented by the small orange spheres.

paths are shown in Fig. 6(c) and (d). For Li₂MnO₃, we observed that the energy barriers for Li diffusion between the 4h site and 2c site are 0.52 and 0.54 eV, aligning well with previous calculations (0.54 and 0.61 eV).³³ For Li hoping between the 4h site

and 2b site, the barriers are 0.57 and 0.70 eV, also consistent with Xiao *et al.*'s calculations.³³ However, after F-doping, the barriers of both paths change significantly. Here, F-doping is modeled by substituting the O site near the Li hoping trajectory

Table 2 Calculated activation barriers (E_a) and estimated diffusion coefficients ($D_{300 \text{ K}}$) for Li₂MnO₃ and Li₂MnO_{2.75}F_{0.25}

Structure	$E_{\rm a}$ (eV)	$D_{300 \text{ K}} (\text{cm}^2 \text{ s}^{-1})$
Li ₂ MnO ₃ Li ₂ MnO _{2.75} F _{0.25}	0.52/0.54/0.57/0.70 0.84/0.56/0.79/0.88	$10^{-11}/10^{-11}/10^{-12}/10^{-14} 10^{-16}/10^{-12}/10^{-15}/10^{-17}$

(Fig. 6(a) and (b)). Although the model is not exhaustive, it provides insights into the effect of F-doping on Li diffusion. As shown in Fig. 6(c) and (d), the path lengths of two pathways are increased after F doping, and E_a increases in both paths after F-doping due to the stronger interaction between F⁻ and Li⁺. The diffusion coefficients of these pathways can be estimated according to $D = d^2v \exp(-E_a/k_bT)$ ($v = 10^{13}$ THz, T = 300 K, and d is the hopping distance)³⁵ as shown in Table 2. Consequently, F-doping leads to a deterioration in the kinetics of Li₂MnO₃.

4. Conclusions

Using the first-principles calculations, we conduct a comprehensive study on the impact of F-doping on the electrochemical performance of Li₂MnO₃. Our results indicate that both Li₂MnO₃ and its F-doped variant, Li₂MnO_{2.75}F_{0.25}, undergo significant volume changes (over 10%) during deep delithiation, which could impede more Li ions cycling of them. Analysis of the electronic structure and magnetic moments in the delithiated states reveals that charge compensation in Li₂MnO₃ primarily involves the oxidation of O²⁻ anions. After F doping, both cationic (Mn) and anionic (O) oxidation are observed in Li₂MnO_{2.75}F_{0.25}, contributing to a lower voltage plateau at the beginning of charge due to the oxidation of Mn³⁺ to Mn⁴⁺, which can somewhat mitigate oxygen release. Additionally, F doping appears to impair Li diffusion kinetics in comparison to pristine Li₂MnO₃, owing to enhanced interactions between F and Li⁺. Our findings offer a deeper insight into the effect of Fdoping on the electrochemical properties of Li₂MnO₃ and provide strategic guidance for future optimization of this highcapacity cathode material.

Data availability

We confirm that the data supporting the finding of this study are available within the main article.

Author contributions

Xiang-Ming Zeng: conceptualization, investigation, formal analysis, writing – original draft, writing – review & editing; Jing Liu: methodology, formal analysis; Jiang-Bin Su: formal analysis, investigation; Fa-Hui Wang, conceptualization, investigation, formal analysis; Yan-Bing Li: methodology; Chang-Jun Zhang: conceptualization; Ming Liu: methodology; Run-Sheng Wu: formal analysis, investigation; Jun-Ping Hu: methodology; Feng Zheng: methodology; investigation, writing – review & editing; supervision.

Conflicts of interest

There are no conflicts to declare.

Acknowledgements

The work at Xinyu University was supported by the Foundation of Jiangxi Province Educational Committee, China (Grant No. GJJ202317) and the Ministry of Education Collaborative Education Project for Industry-University Cooperation (Grant No. 231103117091418). The work at Jimei University was supported by the Natural Science Foundation of Xiamen, China (Grant No. 3502Z202372015), the Fujian Provincial Education Department, China (Grant No. JZ230025) and the Research Foundation of Jimei University (Grant No. ZQ2023013).

References

- 1 J. B. Goodenough and K.-S. Park, *J. Am. Chem. Soc.*, 2013, **135**, 1167–1176.
- 2 M. Sathiya, G. Rousse, K. Ramesha, C. Laisa, H. Vezin, M. T. Sougrati, M.-L. Doublet, D. Foix, D. Gonbeau and W. Walker, *Nat. Mater.*, 2013, 12, 827–835.
- 3 J. Lee, A. Urban, X. Li, D. Su, G. Hautier and G. Ceder, *Science*, 2014, 343, 519–522.
- 4 K. G. Gallagher, S. Goebel, T. Greszler, M. Mathias, W. Oelerich, D. Eroglu and V. Srinivasan, *Energy Environ. Sci.*, 2014, 7, 1555–1563.
- 5 M. S. Whittingham, Chem. Rev., 2004, 104, 4271-4302.
- 6 M. M. Thackeray, C. S. Johnson, J. T. Vaughey, N. Li and S. A. Hackney, *J. Mater. Chem.*, 2005, **15**, 2257–2267.
- 7 T. Ohzuku, M. Nagayama, K. Tsuji and K. Ariyoshi, *J. Mater. Chem.*, 2011, 21, 10179–10188.
- 8 D. H. Seo, J. Lee, A. Urban, R. Malik, S. Kang and G. Ceder, Nat. Chem., 2016, 8, 692–697.
- W. He, W. Guo, H. Wu, L. Lin, Q. Liu, X. Han, Q. Xie, P. Liu,
 H. Zheng and L. Wang, Adv. Mater., 2021, 33, 2005937.
- 10 F. Zheng, S. Y. Zheng, P. Zhang, X. F. Zhang, S. Q. Wu, Y. Yang and Z. Z. Zhu, J. Phys. Chem. C, 2019, 123, 13491– 13499.
- 11 G. Assat and J.-M. Tarascon, Nat. Energy, 2018, 3, 373-386.
- 12 R. A. House, G. J. Rees, M. A. Pérez-Osorio, J.-J. Marie, E. Boivin, A. W. Robertson, A. Nag, M. Garcia-Fernandez, K.-J. Zhou and P. G. Bruce, *Nat. Energy*, 2020, 5, 777–785.
- 13 R. A. House, J.-J. Marie, M. A. Pérez-Osorio, G. J. Rees, E. Boivin and P. G. Bruce, *Nat. Energy*, 2021, 6, 781–789.
- 14 S. Hu, A. S. Pillai, G. Liang, W. K. Pang, H. Wang, Q. Li and Z. Guo, *Electrochem. Energy Rev.*, 2019, 2, 277–311.
- E. Wang, D. Xiao, T. Wu, X. Liu, Y. Zhou, B. Wang, T. Lin,
 X. Zhang and H. Yu, Adv. Funct. Mater., 2022, 32, 2201744.
- 16 L. Zeng, H. Liang, B. Qiu, Z. Shi, S. Cheng, K. Shi, Q. Liu and Z. Liu, Adv. Funct. Mater., 2023, 33, 2213260.
- 17 J. Huang, B. Ouyang, Y. Zhang, L. Yin, D.-H. Kwon, Z. Cai, Z. Lun, G. Zeng, M. Balasubramanian and G. Ceder, *Nat. Mater.*, 2023, 22, 353–361.

- 18 Y. Wang, H.-T. Gu, J.-H. Song, Z.-H. Feng, X.-B. Zhou, Y.-N. Zhou, K. Wang and J.-Y. Xie, J. Phys. Chem. C, 2018, 122, 27836-27842.
- 19 P. Vanaphuti, J. Bai, L. Ma, S. Ehrlich, K. Kisslinger, F. Wang and Y. Wang, Energy Storage Mater., 2020, 31, 459-469.
- 20 D. Mao, X. Tan, Z. Fan, L. Song, Y. Zhang, P. Zhang, S. Su, G. Liu, H. Wang and W. Chu, ACS Appl. Mater. Interfaces, 2023, 15, 10774-10784.
- 21 G. Kresse and D. Joubert, Phys. Rev. B: Condens. Matter Mater. Phys., 1999, 59, 1758-1775.
- 22 G. Kresse and J. Furthmuller, Phys. Rev. B: Condens. Matter Mater. Phys., 1996, 54, 11169-11186.
- 23 G. Kresse and J. Furthmuller, Comput. Mater. Sci., 1996, 6, 15-50.
- 24 J. P. Perdew, K. Burke and M. Ernzerhof, Phys. Rev. Lett., 1996, 77, 3865-3868.
- 25 S. L. Dudarev, G. A. Botton, S. Y. Savrasov, C. J. Humphrevs and A. P. Sutton, Phys. Rev. B: Condens. Matter Mater. Phys., 1998, 57, 1505-1509.

- 26 F. Zhou, M. Cococcioni, C. A. Marianetti, D. Morgan and G. Ceder, Phys. Rev. B: Condens. Matter Mater. Phys., 2004, 70, 235121.
- 27 Y. Koyama, I. Tanaka, M. Nagao and R. Kanno, J. Power Sources, 2009, 189, 798-801.
- 28 H. J. Monkhorst and J. D. Pack, Phys. Rev. B: Solid State, 1976, 13, 5188-5192.
- 29 L. Wang, T. Maxisch and G. Ceder, Phys. Rev. B: Condens. Matter Mater. Phys., 2006, 73, 195107.
- 30 G. Henkelman, B. P. Uberuaga and H. Jónsson, J. Chem. Phys., 2000, 113, 9901-9904.
- 31 X. Zhang, F. Zheng, S. Wu and Z. Zhu, Phys. Chem. Chem. Phys., 2021, 23, 4829-4834.
- 32 Y. Xiang and X. Wu, Ionics, 2018, 24, 83-89.
- 33 R. J. Xiao, H. Li and L. O. Chen, Chem. Mater., 2012, 24, 4242-4251.
- 34 H. Chen and M. S. Islam, Chem. Mater., 2016, 28, 6656-6663.
- 35 R. Kutner, Phys. Lett. A, 1981, 81, 239-240.